LETTER

Designing reversible multi-level resistance states in a half-doped manganite

A Letters Journal Exploring the Frontiers of Physics

January 2021

EPL, **133** (2021) 17006
doi: 10.1209/0295-5075/133/17006

www.epljournal.org

Designing reversible multi-level resistance states in a half-doped manganite

Sanjib Banik, Kalipada Das, Kalpataru Pradhan[a] and Indranil Das[b]

CMP Division, Saha Institute of Nuclear Physics - Kolkata 700064, India

received 30 September 2020; accepted in final form 7 December 2020
published online 5 March 2021

PACS 75.47.-m – Magnetotransport phenomena; materials for magnetotransport

Abstract – We design reversible multi-level resistance states in a half-doped charge-ordered manganite, $Sm_{0.5}Ca_{0.25}Sr_{0.25}MnO_3$ (SCSMO). By exploiting the electronic phase separation in SCSMO at 10 K, we show that the system can be stabilized into several metastable states, against thermal cycling, up to 62 K. The magnetization and the resistivity remain unaltered in each metastable states during the thermal cycling. Monte Carlo calculations using a two-band double-exchange model, including super-exchange, electron-phonon coupling, and quenched disorder, show that the system freezes into a phase-separated metastable state due to the disorder during the thermal cycling. We outline pathway to control the multi-level switching between four reversible metastable states. Our results may open the door for future investigations to engineer memory devices based on multi-level resistance switching using phase-separated transition metal oxides.

Introduction. – Fabrication of non-volatile memory (NVM) devices with high storage density, fast switching speed and low power consumption is of current research interest [1–5]. Recently, random access memory (RAM), based on resistive switching (RS) phenomenon [6–10], has emerged as a new candidate to design functional NVM devices. A typical resistive memory device uses two resistive states to store binary digits 0 and 1. Such memory devices based on resistive switching between two states face scaling issues to deal with next-generation computing systems [11].

A promising but challenging direction to overcome the scaling issues is to design multi-bit memory devices where the intermediate resistivity states can also be used to store digital data. For example a four-level resistive system can store two-bit data (00 or 01 or 10 or 11) in each chips as compared to one-bit data (0 or 1) in a two-level resistive system. The feasibility of multi-level cell has been investigated earlier for phase change memory (PCM) in chalogenides [12–16]. In PCM cells the crystallinity is controlled to obtain different resistance states. In spite of having tremendous functionality, the elemental segregation upon repeated thermal cycling remains a major drawback for PCM cells [17–22]. In this context, the obvious question arises: can one design multiple resistance states by controlling the electronic phases, seen in phase-separated transition metal oxides [23–29] that do not have the problem of elemental segregation?

In this paper, we establish a pathway to design reversible multi-level resistive systems by tuning the electronic phase competition in a half-doped manganite. Recently we have shown that the charge-ordered antiferromagnetic insulating (CO-AFM-I) state, in a $Sm_{0.5}Ca_{0.25}Sr_{0.25}MnO_3$ (SCSMO) sample, melts to a ferromagnetic (FM) metallic state at a moderate critical magnetic field ∼4.5 T [30] at 10 K and remains in a phase coexisting metallic state even after the removal of the magnetic field. In this work we cooled the sample to 10 K and applied a 7 T magnetic field (in principle any field value above the critical field ∼4.5 T can be applied) followed by the zero field warming. The resistivity increases up to ∼65 K and decreases thereafter. Rather than increasing the temperature continuously, during the zero field warming, we stop at four representative temperatures (35 K, 45 K, 52 K, 58 K) and perform temperature cycling between each representative temperatures and 10 K. The distinctly different magnetization and resistivity data generated at above four representative temperatures remains more or less unchanged during the temperature cycling. Then, we show that these metastable states are reproducible. Our Monte Carlo calculations

[a]E-mail: kalpataru.pradhan@saha.ac.in (corresponding author)
[b]E-mail: indranil.das@saha.ac.in (corresponding author)

using two-band double-exchange model verifies that the system freezes to a metastable phase during the thermal cycling and attributes it to the pinning of magnetization at atomic-level chemical disorder that is in built in the system due to radii mismatch between different A-type (Sm, Ca, Sr) ions. So our joint study displays how the electronic phase competition can be tuned in a controllable manner. In addition, we demonstrate the multi-level switching effect between the metastable states.

Magnetic and magnetotransport measurements. – We prepared a high-quality polycrystalline $Sm_{0.5}Ca_{0.25}Sr_{0.25}MnO_3$ (SCSMO) sample using well-known sol-gel technique [30–32] (please see the Supplementary Material `Supplementarymaterial.pdf` (SM) for details). It is known that the electrical resistance in manganite is controlled by the magnetic property [33–36]. In order to gain a deeper understanding about the magnetic properties magnetization measurements were performed using different protocols. Figure 1(a) shows the magnetization (M) *vs.* temperature (T), measured in the presence of 0.01 T external magnetic field for SCSMO (and $Sm_{0.5}Ca_{0.5}MnO_3$ (SCMO)) using zero field cooled warming (ZFCW), field cooled cooling (FCC), and field cooled warming (FCW) protocols. FCW curve in both SCSMO and SCMO exactly overlay on the FCC curve. The bifurcation between ZFCW and FCW curves in SCSMO as well as the peak in ZFCW indicate that small but finite ferromagnetically oriented fractions are induced even for 0.01 T external magnetic field in SCSMO which is practically absent in SCMO. This is due to the substitution of larger Sr ions in place of Ca in the parent compound $Sm_{0.5}Ca_{0.5}MnO_3$ [30]. The dip in the $d\log(M)/dT$ *vs.* T curve for SCSMO (see the inset of fig. 1(a)) also substantiates the presence of the induced ferromagnetic fractions below 62 K. Along with the ferromagnetic transition the inset also depicts an antiferromagnetic transition (T_N) at 110 K and a charge-ordered transition (T_{CO}) around 190 K. Temperature dependence of activation energy (see ref. [30]) also confirms these two transition temperatures (T_N and T_{CO}). To substantiate it further we plot the magnetization *vs.* temperature in 0.1 T external magnetic field for SCSMO (see fig. 1(b)). Obviously the amount of ferromagnetically oriented fractions is enhanced in 0.1 T (as compared to the 0.01 T case), but the transition temperatures remain more or less the same as shown in fig. 1(b). This validates the antiferromagnetic and charge-ordered transitions in SCSMO. All these results signify the presence of phase coexistence at low temperatures.

To further study the phase coexistence in SCSMO, we apply 3.5 T magnetic field and measure M *vs.* T using three (ZFCW, FCW, and FCC) protocols, as shown in fig. 1(c). Here the ZFCW curve also shows a maximum around 60 K similar to ZFCW curve in 0.01 T magnetic field. For SCSMO, 3.5 T magnetic field melts the CO-AFM-I state to FM metallic state although

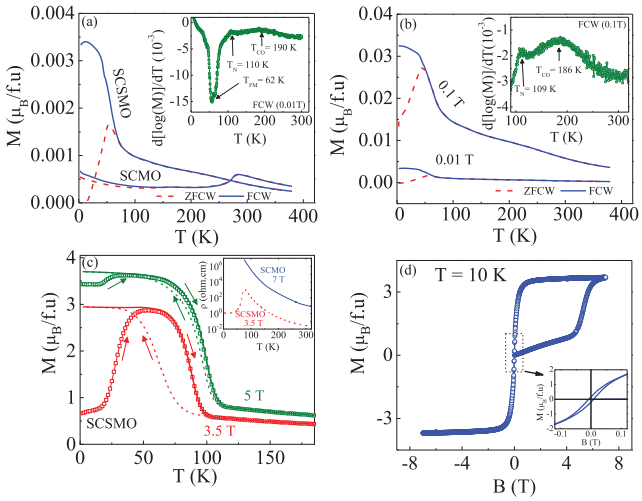

Fig. 1: Magnetic properties of SCSMO: temperature dependence of magnetization measured in the presence of (a) 0.01 T and (b) 0.1 T magnetic field using ZFCW (dashed line) and FCW (solid line) protocols. Magnetization *vs.* temperature for SCMO (using 0.01 T in (a)) and for SCSMO (using 0.01 T in (b)) are also plotted for comparison. Different transition temperatures in 0.01 T are marked by the arrows (T_{CO} = 190 K, T_N = 110 K and T_{FM} = 62 K) for SCSMO in the inset of (a). T_{CO} and T_N in 0.1 T are also indicated in the inset of (b). (c) Magnetization with temperature for 3.5 T and 5 T magnetic fields (dotted line, solid line and line with square symbols indicate the FCC, FCW and ZFCW magnetization data, respectively). Inset in (c) shows resistivity *vs.* temperature for SCMO (at 7 T) and SCSMO (at 3.5 T). (d) Magnetization *vs.* magnetic field at 10 K for SCSMO. Inset shows the zoomed curve.

7 T magnetic field had no effect on the parent compound SCMO (see the inset for resistivity comparison). The moderate hysteresis between the FCC and the FCW measurements in 3.5 T indicates the phase coexistence between the FM and The AFM phases over the temperature range 50–100 K, but the phase coexistence diminishes for 5 T magnetic field (see fig. 1(c)). In addition, we plot the magnetization *vs.* magnetic field isotherms at 10 K, in fig. 1(d). Interestingly it shows that there is a small but finite remnant magnetization after the removal of the field.

Observation of multi-level resistance states. – In order to explore the evolution of phase coexistence in SCSMO with the temperature, we measure M *vs.* T and ρ *vs.* T using different protocols. Initially we cooled the system from 300 K to 10 K. For magnetization measurements a test field (0.01 T) is always applied unless otherwise specified. Magnetization at 10 K remains very small ($<10^{-2}\,\mu_B$/f.u) and resistivity is found to be insulating in nature (see fig. 2(a) and (b)). At this point, we apply and then remove the 7 T magnetic field, and record the magnetization (the resistivity) data while increasing the temperature (defined as ZFW-I) as shown in fig. 2(a) and (b). We find that the remnant magnetization ($0.33\,\mu_B$/f.u

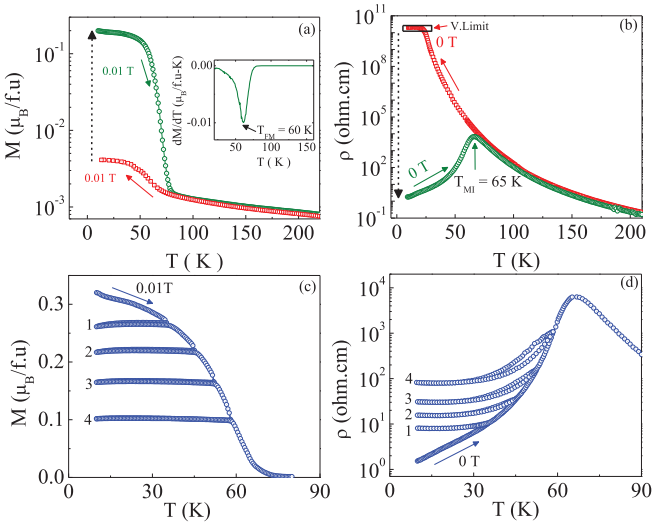

Fig. 2: Multi-level resistive states in SCSMO: (a) square symbols (FCC): temperature dependence of the magnetization in the 0.01 T magnetic field. Open circle symbols (ZFW-I): variation of magnetization with temperature in the 0.01 T magnetic field (after applying and removing 7 T magnetic field at 10 K). The inset shows the temperature derivative of $M(T)$ data taken during the warming process. (c) Similar to ZFW-I, but temperature cycling down to 10 K was performed while increasing the temperature at four representative temperature points (defined as ZFW-II). Resistivity corresponding to magnetization data in (a) and (c) are plotted in (b) and (d), respectively. V-limit is the limiting value of our measuring instruments (see the SM for details).

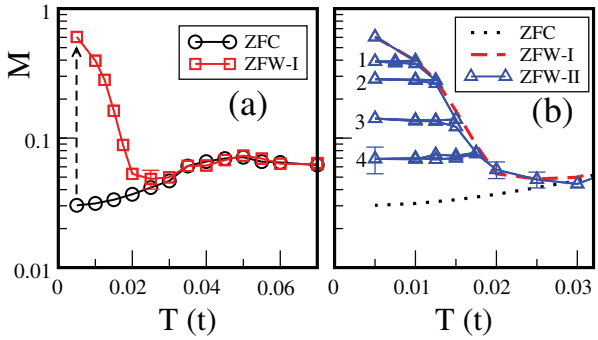

Fig. 3: Monte Carlo results: (a) magnetization *vs.* temperature for ZFC and ZFW-I (with $h = 0$) protocols. Dashed arrow (connecting ZFC and ZFW-I) indicates application and removal of magnetic field $h = 0.2$ at $T = 0.005$. Magnetization data calculated using ZFW-I (using $h = 0$) protocol is also plotted in (b) for comparison. (b) Temperature dependence of magnetization using ZFW-II protocol. Temperature cyclings are performed at four representative temperatures ($T = 0.01$ (state 1), 0.0125 (state 2), 0.015 (state 3), 0.0175 (state 4)). Error bars are given wherever necessary. Error bars at all temperatures in state 4 are more or less the same. So, the error bar is given only at $T = 0.005$ in state 4 for brevity.

at 10 K) decreases with increasing temperature. Correspondingly the resistivity increases with increasing the temperature up to 65 K and decreases thereafter. This temperature is very close to the T_{FM} of SCSMO in 0.01 T magnetic field (see fig. 1(a)). These results suggest that the phase coexistence developed in the system at 10 K, due to the application and removal of the 7 T field, persists up to ∼65 K.

Can one design multiple resistance states by utilizing the phase coexistence in manganites? To answer this we carried out the magnetization measurements following a second protocol (ZFW-II) and were able to unearth the multi-level resistance states. In this particular protocol rather than warming the sample continuously from 10 K to 200 K we heated the sample up to 35 K and performed the temperature cycling between 35 and 10 K as shown in fig. 2(c) (indicated by state 1). Thermoremanent magnetization measured during this process shows that magnetization initially decreases with the heating (from 10 K to 35 K), but the system does not recover the previous magnetization during the recooling process (from 35 K to 10 K). In fact, the magnetization remains constant during the temperature cycling (*i.e.*, during the recooling and the subsequent reheating process). This is unlike the bulk ferromagnet but very similar to the thermal hysteresis obtained for iron-nitride fine particles and CuMn alloys [37] where metastability of the system plays an important role. After the temperature cycling we further increased the temperature from 35 K up to 45 K and repeated the temperature cycling (indicated by state 2). Similarly we performed temperature cycling at 52 K and 58 K indicated by state 3 and state 4, respectively. During the temperature cycling, from 35 K, 45 K, 52 K, and 58 K to 10 K, the magnetization remains unchanged. We also performed the resistivity measurements using the same protocol (see fig. 2(d)) and there is a one-to-one correspondence between the magnetization and the resistivity data. The experimental data of both magnetization and resistivity for the sweep rate dependence, effect of repeated cycling, time dependence, reproducibility of multi-level resistance states (given in the SM) shows that the generated four resistance states are robust by its design. Not only four but a large number of resistance states can be designed using the same protocol. Multi-level resistance states can be used to design multi-level cells for future spintronic applications. For that the system must show reversible multi-level switching effect between the resistance states. Before we present our result on the reversible switching effect we want to uncover the physical origin of these multi-level resistance states.

Physical origin of multi-level resistance states. – During the temperature cycling, say between 35 K to 10 K (see fig. 2(c)), it appears that the size of the ferromagnetic regions freezes in a metastable state [37] and as a result the magnetization remains the same. In order to verify the presence of the metastable states we study a standard two-band model Hamiltonian for the manganites in 2D. Due to the octahedral crystal field splitting the Mn t_{2g} levels have lower energy than the e_g levels and the itinerant e_g electrons are coupled with the t_{2g} electrons (t_{2g} form the

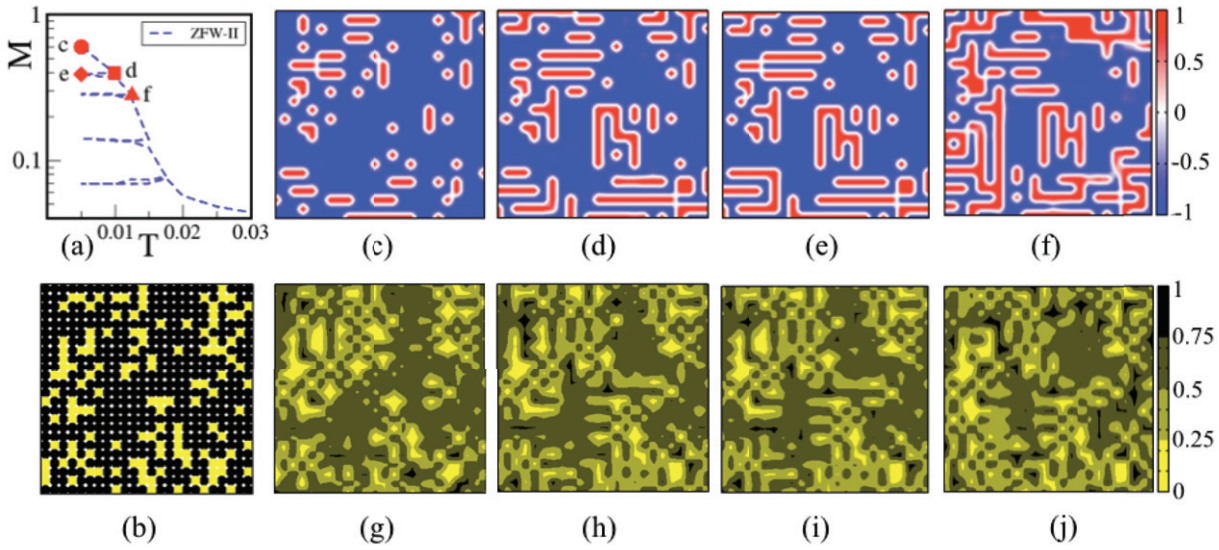

Fig. 4: (a) ZFW-II data from fig. 3(b) is reproduced here highlighting four temperature points using four different symbols; (b) disorder distribution (ϵ_i distribution) for one copy of disorder. Black (yellow) points represent $\epsilon_i = -0.3$ ($\epsilon_i = 0.3$). (c)–(f) The z components of simulated Mn (t_{2g}) spins at each sites. (g)–(j) Corresponding electron density at each sites on a 24×24 lattice using one of the disorder configuration (shown in (b)). (g) is the corresponding electron density for (c), (h) is the corresponding electron density for (d) and so on. The color bar (right of (f)) is for (c)–(f) and the color bar (right of (j)) is for (g)–(j).

core Mn spins S (=3/2)) via large Hund's coupling. The e_g electrons are also coupled to the Jahn-Teller phonons with a coupling strength λ. In addition, antiferromagnetic superexchange interaction J between neighboring core Mn spins is taken into account. This well-investigated Hamiltonian in the double-exchange limit [34] reproduces the phase diagram of manganites [38–40]. In SCSMO, Sr^{2+} ions (larger in size as compared to Sm^{3+} and Ca^{2+} ions) occupy the A-sites randomly and create chemical disorder at the atomic level. In order to incorporate this disorder $\sum_i \epsilon_i n_i$ is added at each Mn site picked from the distribution $P(\epsilon_i) = \frac{1}{4}\delta(\epsilon_i - \Delta) + \frac{3}{4}\delta(\epsilon_i + \Delta)$, where Δ is the disorder potential. In an external magnetic field h, a Zeeman coupling term $-\sum_i \mathbf{h}\cdot\mathbf{S}_i$ is added to the Hamiltonian, where $\mathbf{S}_i$ denotes the classical Mn t_{2g} spin. We use spin-fermion Monte Carlo (MC) technique based on the travelling cluster approximation [41,42] (TCA) for 24×24 lattice (see the SM for details). We ensured that the system is well annealed (using 10^4 Monte Carlo system sweeps in general) at each temperature.

We measure λ, J, Δ, h and T (temperature) in units of kinetic hopping parameter t. The estimated value of t in manganites is 0.2 eV [34]. We use $J = 0.1$, $\lambda = 1.65$ and $\Delta = 0.3$ for SCSMO [30]. Magnetization $(= (S(\mathbf{q}))^{0.5}$ at wave vector $\mathbf{q} = (0, 0)$, where $S(\mathbf{q})$ is the magnetic structure factor $= \frac{1}{24^2}\sum_{ij} \mathbf{S}_i \cdot \mathbf{S}_j \; e^{i\mathbf{q}\cdot(\mathbf{r}_i - \mathbf{r}_j)})$ is averaged over ten different disorder configurations in addition to the thermal averages obtained during the Monte Carlo simulations.

Initially we cooled the system (from $T = 0.1$ to $T = 0.005$) and the corresponding temperature dependence of the magnetization (M) for electron density $n = 1 - x = 0.5$ is shown in fig. 3(a) using open circle symbols. At $T = 0.005$, we apply and remove the external magnetic field ($h = 0.2$). The magnetization of the system drops to 0.6 from 1 upon removal of the field. The temperature dependence of magnetization after removing the magnetic field at $T = 0.005$ (defined as ZFW-I) is shown by the square symbol in fig. 3(a). In the second protocol (ZFW-II), similar to our experiment, after removing the field at $T = 0.005$, we increase the temperature only up to 0.01 and perform a temperature cycling below it (*i.e.*, system is cooled to $T = 0.005$ and then heated up to $T = 0.01$) as represented by state 1 in fig. 3(b)). The magnetization remains unchanged during the temperature cycle. Then from $T = 0.01$ we further increase the temperature to 0.0125 and perform a temperature cycling below it. Similarly system is recycled to lower temperature from $T = 0.015$ and $T = 0.0175$. In all cases the magnetization remains unchanged during the temperature cycling. So, our Monte Carlo calculations systematically reproduce the experimental results.

We move now to analyze the phase coexistence of ferromagnetic-metallic and charge-ordered insulating phases using Monte Carlo snap-shots. Figure 4(a) shows magnetization data using ZFW-II protocol (shown in fig. 3(b)) indicating four representative points. Figures 4(c)–(f) and figs. 4(g)–(j) show the z components of t_{2g} spins and electron density for each sites for a disorder configuration, respectively. Figure 4(b) shows ϵ_i distribution for that disorder configuration. At $T = 0.005$ (after applying and removing $h = 0.2$) the system consists of ferromagnetic metallic and charge-ordered insulating (see fig. 4(c) and (g)) phases. The electron

density is more or less homogeneous (∼0.65) within the ferromagnetic clusters and charge ordered (short range) elsewhere. Comparing with the impurity locations (fig. 4(b)) it is apparently clear that the ferromagnetic-metallic clusters are within the homogeneously distributed ϵ_i regions and are pinned to the disorder configuration. This is the reason for which the magnetization remains finite even after removing the magnetic field. The size of the ferromagnetic-metallic clusters decreases in size with temperature as shown in fig. 4(d) and (h). Interestingly going from T = 0.005 to $T = 0.01$ (*i.e.*, from fig. 4(c) to fig. 4(d)) the magnetic regions get depleted but the remnant ferromagnetic regions at $T = 0.01$ are always part of the bigger ferromagnetic regions seen in $T = 0.005$. During the temperature cycling from $T = 0.01$ to $T = 0.005$ (*i.e.*, state 1) the ferromagnetic regions (compare fig. 4(d) and (e)) get pinned in a metastable state due to the disorder configuration (shown in fig. 4(b)) and as a result magnetization remains the same. For $T = 0.0125$ the ferromagnetic regions (see fig. 4(f) and (j)) further shrink in size and the magnetization decreases further.

Reversible multi-level switching effect. – Next, we show the multi-level switching effect using four-level metastable states. For this, we followed the sequence as shown in fig. 2(a), *i.e.*, cooled the sample down to 10 K followed by the application and removal of 7 T external magnetic field. After that, we increased the temperature to 52 K directly (*i.e.*, going to state 3 directly) as shown in fig. 5. Magnetization data from the thermal cycling at 52 K follows the same path as shown in fig. 2(c). To access another metastable state (say state 2) first we apply and remove 7 T magnetic field at 10 K of state 3. Secondly, we increase the temperature up to 45 K (*i.e.*, state 2) and perform a thermal cycling. The magnetization reproduces the same value that we obtained during ZFW-II process. This step-by-step procedure establishes a concrete way obtain the switching effect between the four metastable states. But, the switching effect in our system is not restricted to four resistance states; in principle more resistance states could be addressed. It is important to note here that on order to construct a multi-bit memory device [43] the system must have at least four reversible resistance states. This is because four states are required to store all possible two-bits (00 or 01 or 10 or 11) data. So we have described a pathway to design multi-level resistance states using phase coexistence in manganites, albeit using temperature probe, which may open the door for future investigations on phase separation to architect memory devices.

We have used a direct temperature probe in our experiments. Temperature probe based on the Joule heating [44], by using voltage pulse, can be used to design such devices. Also, the electronic phase separation (and in turn resistive states) can be controlled by numerous ways like, applying substrate strain, pressure and electric field, using mode-selective vibrational excitations and photo-induction [45–50], etc. We believe that the phase separation scenario in correlated materials using different probes to engineer multi-level resistance switching deserves further investigation. We leave this as the subject for future work.

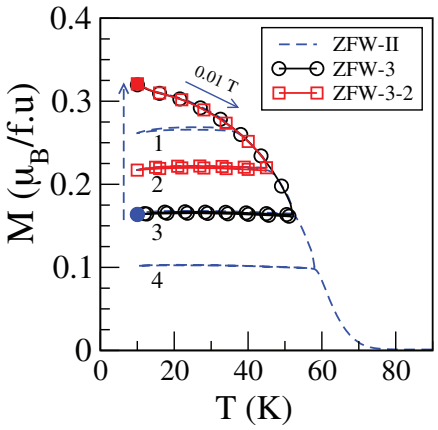

Fig. 5: Multi-level switching: Dashed line is using ZFW-II data reproduced from fig. 2(c). From 10 K we go to 52 K (without any temperature cycling at 35 K and 45 K) and perform temperature cycling (*i.e.*, going to state 3 directly, see ZFW-3). New state 3 data perfectly matches with the state 3 data of ZFW-II. At $T = 10$ K of new state 3 we apply and remove 7 T magnetic field (*i.e.*, going from filled circle symbol to filled square symbol, indicated by an arrow) and then increase the temperature to 45 K. After that we perform a temperature cycling below 45 K (see ZFW-3-2). The magnetization data from new state 2 also matches well with the state 2 data of ZFW-II. A test field (0.01 T) is always applied unless otherwise specified during the magnetization measurement.

Conclusion. – In summary, we combined experimental and theoretical study to outline a simple pathway to design reversible multi-level resistance states. By introducing electronic phase coexistence in a controllable manner in SCSMO, we demonstrated that the system can be stabilized into several metastable states, against thermal cycling, up to 62 K. The magnetization and resistivity data generated at different metastable states remains unchanged during the temperature cycling. By performing Monte Carlo calculations using a two-band double-exchange model we established that the system freezes to a metastable phase during the thermal cycling due to the pinning of magnetization at the atomic-level chemical disorder that is inbuilt in the system due to radii mismatch between different A-type (Sm, Ca, Sr) ions. In the end, we outlined a pathway to achieve multi-level switching between the metastable states. We expect that our results will motivate experimenters to further explore the electronic phase separation in oxides to engineer multi-level resistive switching devices.

* * *

The work was supported by Department of Atomic Energy (DAE), Government of India. We acknowledge

the use of MEGHNAD and MEGHNAD2019 computer clusters at SINP. We thank Sudhakar Yarlagadda for his comments on the manuscript.

Data availability statement: The data that support the findings of this study are available from the corresponding author upon reasonable request.

REFERENCES

[1] Scott J. C., *Science*, **304** (2004) 62.
[2] Meijer G. I., *Science*, **319** (2008) 1625.
[3] Chen X., Wu G. and Baoa D., *Appl. Phys. Lett.*, **93** (2008) 093501.
[4] Pan F., Chen C., Wang Z., Yang Y., Yang J. and Zeng F., *Prog. Nat. Sci.: Mater. Int.*, **20** (2010) 1.
[5] Hwang C. S., *Adv. Electron. Mater.*, **1** (2015) 6.
[6] Sawa A., *Mater. Today*, **11** (2008) 28.
[7] Jeong D. S., Thomas R., Katiyar R. S., Scott J. F., Kohlstedt H., Petraru A. and Hwang C. S., *Rep. Prog. Phys.*, **75** (2012) 076502.
[8] Kim S., *Sci. Rep.*, **3** (2013) 1680.
[9] Ielmini D., *Semicond. Sci. Technol.*, **31** (2016) 063002.
[10] Russo P., Xiao M., Liang R. and Zhou N. Y., *Adv. Funct. Mater.*, **28** (2018) 1706230.
[11] Wang M., Lv H., Liu Q., Li Y., Xu Z., Long S., Xie H., Zhang K., Liu X., Sun H., Yang X. and Liu M., *IEEE Electron Device Lett.*, **33** (2012) 11.
[12] Wuttig M. and Yamada N., *Nat. Mater.*, **6** (2007) 824.
[13] Koelmans W. W., Sebastian A., Jonnalagadda V. P., Krebs D., Dellmann L. and Eleftheriou E., *Nat. Commun.*, **6** (2015) 8181.
[14] Wang L., Tu L. and Wen J., *Sci. Technol. Adv. Mater.*, **18** (2017) 406.
[15] Salinga M., Kersting B., Ronneberger I., Jonnalagadda V. P., Vu X. T., Gallo M. L., Giannopoulos I., Miredin O. C., Mazzarello R. and Sebastian A., *Nat. Mater.*, **17** (2018) 681.
[16] Xie Y., Kim W., Kim Y., Kim S., Gonsalves J., BrightSky M., Lam C., Zhu Y. and Cha J. J., *Adv. Mater.*, **30** (2018) 1705587.
[17] Raoux S., Jordan-Sweet J. L. and Kellock A. J., *J. Appl. Phys.*, **103** (2008) 114310.
[18] Raoux S., Cheng H. Y., Jordan-Sweet J. L., Munoz B. and Hitzbleck M., *Appl. Phys. Lett.*, **94** (2009) 183114.
[19] Beneventi G. B., Calderoni A., Fantini P., Larcher L. and Pavan P., *J. Appl. Phys.*, **106** (2009) 054506.
[20] Simpson R. E., Krbal M., Fons P., Kolobov A. V., Tominaga J., Uruga T. and Tanida H., *Nano Lett.*, **10** (2010) 414.
[21] Boniardi M. and Ielmini D., *Appl. Phys. Lett.*, **98** (2011) 243506.
[22] Chen B., Ten Brink G. H., Palasantzas G. and Kooi B. J., *Sci. Rep.*, **6** (2016) 265.
[23] Asamitsu A., Tomioka Y., Kuwahara H. and Tokura Y., *Nature*, **388** (1997) 3.
[24] Uehara M., Mori S., Chen C. H. and Cheong S. W., *Nature*, **399** (1999) 10.
[25] Ahn K. H., Lookman T. and Bishop A. R., *Nature*, **428** (2004) 25.
[26] Sarma D. D., Topwal D., Manju U., Krishnakumar S. R., Bertolo M., Rosa S. L., Cautero G., Koo T. Y., Sharma P. A., Cheong S.-W. and Fujimori A., *Phys. Rev. Lett.*, **93** (2004) 097202.
[27] Odagawa A., Sato H., Inoue I. H., Akoh H., Kawasaki M., Tokura Y., Kanno T. and Adachi H., *Phys. Rev. B*, **70** (2004) 224403.
[28] Rubi D., Tesler F., Alposta I., Kalstein A., Ghenzi N., Gomez-Marlasca F., Rozenberg M. and Levy P., *Appl. Phys. Lett.*, **103** (2013) 163506.
[29] Hoffman J. D., Wu S. M., Kirby B. J. and Bhattacharya A., *Phys. Rev. Appl.*, **9** (2018) 044041.
[30] Banik S., Das K., Paramanik T., Lalla N. P., Satpati B., Pradhan K. and Das I., *NPG Asia Mater.*, **10** (2018) 923.
[31] Venkataiah G. and Venugopal Reddy P., *J. Magn. & Magn. Mater.*, **285** (2005) 343.
[32] Banik S. and Das I., *J. Alloys Compd.*, **742** (2018) 248.
[33] Kuwahara H., Tomioka Y., Asamitsu A., Moritomo Y. and Tokura Y., *Science*, **270** (1995) 961.
[34] Dagotto E., Hotta T. and Moreo A., *Phys. Rep.*, **344** (2001) 1.
[35] Salamon M. B. and Jaime M., *Rev. Mod. Phys.*, **73** (2001) 583.
[36] Tokura Y., *Rep. Prog. Phys.*, **69** (2006) 797.
[37] Mamiya H., Nimori S., Ohnuma M., Nakatani I., Demura M. and Furubayashi T., *J. Magn. & Magn. Mater.*, **316** (2007) 535.
[38] Yunoki S., Moreo A. and Dagotto E., *Phys. Rev. Lett.*, **81** (1998) 5612.
[39] Pradhan K., Mukherjee A. and Majumdar P., *EPL*, **84** (2008) 37007.
[40] Pradhan K. and Yunoki Y., *Phys. Rev. B*, **96** (2017) 214416.
[41] Kumar S. and Majumdar P., *Eur. Phys. J. B*, **50** (2006) 571.
[42] Pradhan K., Mukherjee A. and Majumdar P., *Phys. Rev. Lett.*, **99** (2007) 147206.
[43] Gajek Martin, Bibes Manuel, Fusil Stephane, Bouzehouane Karim, Fontcuberta Josep, Barthelemy Agnes and Fert Albert, *Nat. Mater.*, **6** (2007) 296.
[44] Lee D. H. and Lim S. H., *Appl. Phys. Lett.*, **92** (2008) 233502.
[45] Gillaspie D., Ma J. X., Zhai H. Y., Ward T. Z., Christen H. M., Plummer E. W. and Shen J., *J. Appl. Phys.*, **99** (2006) 08S901.
[46] Elovaara T., Majumdar S., Huhtinen H. and Paturi P., *Adv. Funct. Mater.*, **25** (2015) 5030.
[47] Chai X., Xing H. and Jin K., *Sci. Rep.*, **6** (2016) 23280.
[48] Rini M., Tobey R., Dean N., Itatani J., Tomioka Y., Tokura Y., Schoenlein R. W. and Cavalleri A., *Nature*, **499** (2007) 72.
[49] Baldini M., Capogna L., Capone M., Arcangeletti E., Petrillo C., Goncharenko I. and Postorino P., *J. Phys.: Condens. Matter*, **24** (2012) 045601.
[50] Garbarino G., Acha C., Levy P., Koo T. Y. and Cheong S. W., *Phys. Rev. B*, **74** (2006) 100401R.